Received: 30 November 2021 | Revised: 24 January 2022 | Accepted: 25 February 2022

DOI: 10.1002/cjce.24544

RESEARCH ARTICLE

THE CANADIAN JOURNAL OF CHEMICAL ENGINEERING

Experiments and simulations of settling cylinders over a wide range of Archimedes numbers

Jinghan Xie[1] | **Lijuan Zhang**[1] | **Menghua Lu**[1] | **Jie Lu**[1] | **Jos J. Derksen**[2]

[1]School of Chemistry and Chemical Engineering, Shanghai University of Engineering Science, Shanghai, China

[2]School of Engineering, University of Aberdeen, Aberdeen, UK

Correspondence
Lijuan Zhang and Jie Lu, School of Chemistry and Chemical Engineering, Shanghai University of Engineering Science, Shanghai, China.
Email: zhanglj0128@126.com and lujie@sues.edu.cn

Funding information
National Natural Science Foundation of China, Grant/Award Numbers: 22078191, 21978165, 22081340412

Abstract

Quantitative visualization experiments and particle-resolved simulations of rigid cylindrical particles settling in a Newtonian liquid have been conducted. By varying the viscosity of the liquid—a glycerol-water mixture—as well as the density of the cylinders, we were able to cover an Archimedes number range that spans almost six orders of magnitude in the experiments. The length over diameter aspect ratio of the cylinders ranged from 2.5 to 20. Cylinders were released vertically and rotated to a stable horizontal orientation in most of the lower viscosity solutions. The time required for reaching a horizontal orientation, as well as the Reynolds number at that stage, scale with the Archimedes number and only weakly depend on the aspect ratio. Particle-resolved numerical simulations based on the lattice-Boltzmann method complement the experimental study and illustrate the relevance of the experimental data as a benchmark for numerical approaches to solid–liquid flow with non-spherical particles.

KEYWORDS

computational fluid dynamics, particle-resolved simulation, sedimentation, solid–liquid flow, visualization experiments

1 | INTRODUCTION

Interaction between solid particles and fluid is at the core of many chemical engineering applications, for example catalytic processes, separation processes such as crystallization, and bioprocess technologies such as wastewater treatment. Settling and suspension of solid particles in fluids is common in nature and industrial production processes. It exists in natural phenomena, for instance, the deposition of substances in rivers, lakes, seas, and the atmosphere, as well as in practical applications in industrial process, such as wastewater treatment, the papermaking process, and food processing.

The research on the sedimentation motion of solid particles in fluids is largely confined to particles of spherical shape.[1–4] Multiphase flow of non-spherical particles in fluids is a strongly developing research topic given its richness of anisotropic phenomena and practical relevance.[5] In the sedimentation process, the largest difference between non-spherical particles and spherical particles is the onset of instabilities related to particle orientation relative to the direction of gravity; for example, particles flipping, tumbling, and swinging.

The starting point for the modelling of solid–fluid systems is the momentum exchange between solids and fluid as a result of their relative motion. As early as 1922, Jeffery[6] carried out theoretical research on non-spherical particles, calculated the resultant force and moment of ellipsoid particles in a Stokes flow field under constant velocity gradient, and deduced the motion formula of ellipsoid particles in simple shear flow. In 1964, Marchildon et al.[7] studied the behaviour of a single

cylinder moving in water under the action of gravity with Reynolds numbers in the range of 70–2400. It was concluded that the drag coefficient of oscillating particles was related to the density of particles and that the oscillation frequency was a computable function of the hydrodynamic force and the inertia of particles. In 1975, Youngren and Acrivos[8] used numerical methods to simulate the Stokes flow field around cylindrical particles and obtain their resistance. In 1993, Loewenberg[9] numerically calculated Stokes drag, added mass and Bassett force of a cylinder with a finite oblong section by using the boundary integral formula. The numerical results of a cylinder moving parallel or perpendicular to its symmetry axis with aspect ratios in the range of 0.01–100 were given. In 2008, Hyensjo and Dahlkild[10] used the Fokker–Planck equation to study the orientation distribution function and rotation-rotation diffusion coefficient of slender particles in a planar contracting flow with different turbulence degrees, and proposed two dimensionless rotational diffusion hypotheses based on two different turbulence time scales.

There are also a large number of experimental studies on non-spherical particles settling in fluids. The classification of the experimentally observed phenomena is of great significance for the future research on the non-spherical particles. In 1986, Chiba et al.[11] studied the movement of a slender cylinder falling in water and in aqueous polyacrylamide and hydroxyethyl cellulose. It was shown that slender objects rotate horizontally in Newtonian liquids and vertically in viscoelastic liquids. The experimental work of Joseph et al.[12,13] reported that the cylinder tilting transition was a phenomenon produced by the competition between viscoelasticity and inertia. The tilt angle could be discussed in terms of a competition between viscous, viscoelastic, and inertial effects. In a purely viscous fluid, only the Reynolds number enters, and inertia always prevails.[13] This implies that no matter how small the Reynolds number is, the cylinder will eventually turn its side towards the flow.

Recently, detailed experimental work on settling cylinders has been reported by Toupoint et al.[14] It focuses on the settling regimes and identifies and quantifies instabilities associated to settling cylinders over a range of Archimedes numbers and length over diameter aspect ratios.

In the current paper, we study the sedimentation of rigid, solid cylinders through a Newtonian liquid over a wide range of Archimedes numbers and aspect ratios. The focus is on building an experimental data base and identifying the key dimensionless parameters that govern the speed and orientation of the cylinders while settling over a wide range of conditions. As an example of the latter, the Archimedes number (Ar) that captures the competition between net gravity and viscous effects has been varied between approximately 1 and 3×10^5.

The experimental work is complemented with numerical simulations based on the lattice-Boltzmann method. Once validated by the experimental data, the simulations provide some more insight in the time scales and flow structures that lead to the evolution of the cylinders' orientation while settling.

The paper starts by defining the flow system and the governing dimensionless numbers. Experimental procedures and methods are discussed next. Then there is a brief outline of the simulation method used. Section 6 starts with impressions of experimental and numerical results. Then numerical results are compared to the experimental ones and a further interpretation of the settling process is given. We finish the paper by summarizing the main conclusions and discussing option for future work.

2 | FLOW SYSTEM

All the experiments were carried out in a rectangular column made of plexiglass with a height of 800 mm and square cross-section with a side length of 80 mm. The column was filled with a Newtonian liquid consisting of a glycerol-water mixture, with density ρ_l and kinematic viscosity ν. In the experiments, cylindrical particles with diameter d, length l and density $\rho_s > \rho_l$ were used. As to the dimensionless input parameters we identified the aspect ratio l/d, the density ratio $\gamma = \rho_s/\rho_l$, and the Archimedes number $\mathrm{Ar} = (\gamma - 1) g d^3/\nu^2$ with g gravitational acceleration. It should be noted that this definition of Ar only considers the diameter d as the length scale. Others[15] involve the length of the cylinder through the equivalent diameter $d_e = \sqrt[3]{3d^2 l/2}$. Also, an Ar defined such that its value is the square root of the values in this paper has been proposed.[14] The reason for us not involving l in the definition of Ar is to stay true to the interpretation of the Archimedes number as a Stokes estimate of the settling Reynolds number. If drag is approximately proportional to l then that settling velocity does not strongly depend on l since also net gravity is proportional to the length.

The cylinders are released vertically at the top of the column, fully submerged in the liquid. When observing the settling of cylinders in the column, three regimes have been identified: (1) the cylinder stays vertical for the duration of the experiment; (2) the cylinder rotates to a horizontal orientation without wobbling; (3) the cylinder wobbles and eventually reaches a horizontal orientation. The two main dimensionless output parameters of the experiments are the Reynolds number based on the speed

at the moment the cylinder gets horizontal for the first time $\mathrm{Re} = |u|d/\nu$ and the dimensionless time from release to first reaching horizontal orientation tv/d^2.

3 | EXPERIMENTAL SETUP

Glycerol-water mixtures were used in the experiment in order to cover a wide range of viscosities—and therefore Archimedes numbers. The experiments were carried out in the winter in east China at a room temperature of 20 ± 1°C. The dynamic viscosity of each mixture used was measured with NDJ-5S rotary viscometer at the same temperature as in the sedimentation experiment. The density of each mixture was measured with a constant volume density bottle. Before each measurement, the instruments were calibrated with a standard liquid. Then the experimental liquids were measured five times, and average values and standard deviations were determined. The kinematic viscosity ν was calculated from the density and the dynamic viscosity. All data for all liquid mixtures used are in Table 1.

We used 28 cylinders made of stainless steel, iron, and copper (of which densities were measured as 7.922, 7.811, and 8.948 g/cm^3, respectively) with lengths ranging from $l = 5.00$ to 29.70 mm, diameters ranging from $d = 1.05$ to 2.99 mm and l/d aspect ratios ranging from 2.54 to 18.88. The mass of each cylinder was weighed by an electronic balance with a measurement error of ±0.01 mg, and the diameter and length was measured by a micrometre with a measurement error of ±0.005 mm. The relevance of studying cylinders of different sizes having (approximately) the same aspect ratio is that they have different Archimedes numbers.

Before the particle settling experiment, the glycerol-water mixture was filled into the settling column and left for 4–12 h depending on glycerol concentration to allow air bubbles to escape and reach thermal equilibrium and to measure the viscosity of the liquid. The cylinders were fully immersed in the glycerol-water mixture before being released to eliminate any possibility of air entrainment. We clamped the tip of the cylinder with tweezers and lowered it slowly into the liquid and held it steady. We then gently loosened the tweezers and the cylinder was released under the liquid surface at the top of the settling column. Their axes were parallel to the axis of the settling column and as close to the centre of the settling column as possible. The settling process was captured by a digital camera, and the video images of the release of the cylinders were checked to ensure that the cylinders were vertical upon release within ±0.5°, and those cases were considered valid. The frame rate of the camera was adjusted according to the settling velocity. Given the frame rate, the position of the centre of gravity of the cylinder as a function of time could be determined.

The particle diameter is less than 4% of the side length of the settling column, and therefore—at least initially—wall effects are considered to be minor. However, when the particle settles and rotates, the distance between a tip of the cylinder and the wall can get relatively small. In case a tip of the cylinder gets in contact with a wall, the experiment was discarded.[16]

4 | EXPERIMENTAL DATA ANALYSIS

As indicated above, the settling process has been filmed with SONY FDR-AX700 digital camera. It has 1920 × 1080 pixels, about 2203 PPI pixel density, and can be operated with a variable frame rate f. The frame rate is set at 50–500 FPS, depending on the settling velocity of cylinders. Each pixel represents a square with side length $\delta = 0.77 \pm 0.01$ mm in the liquid column. The two main output parameters of each experiment are (1) the time from release to the moment a cylinder is horizontally oriented for the first time and (2) the vertical velocity at that moment. The uncertainty in the time-to-horizontal, therefore, is the time between frames $1/f$. The frame rate is adjusted such that the relative error in the time-to-horizontal is 8% or less.

TABLE 1 Settling fluid density and viscosity data at 20 ± 1°C

Glycerin concentration (by volume) (%)	Density ρ_l (g/cm^3)	Standard deviation $\sigma(\rho_l)$ (g/cm^3)	Dynamic viscosity μ (mPa · s)	Standard deviation $\sigma(\mu)$ (mPa · s)	Kinematic viscosity ν (10^{-6} m^2/s)
100	1.261	0.010	1251.2	60.0	992.2
95	1.260	0.0068	493.0	37.8	391.3
80	1.193	0.011	87.40	18.2	73.26
60	1.143	0.0057	16.40	1.15	14.35
40	1.104	0.0070	6.40	0.099	5.80
20	1.052	0.0060	2.48	0.033	2.36

Once the image frame that has the cylinder closest to horizontal has been identified, we determine the vertical coordinate z_1 of the centre of gravity of the cylinder n frames back and the vertical coordinate z_2 with m frames forth and then determine the velocity as $|u| = (z_1 - z_2)f/(n+m)$. The main uncertainty in this velocity determination is the pixelation of the camera frames that, given that we subtract two z -values, is estimated as two times the size of a pixel $2\delta = 1.5$ mm. Frame rate f and numbers of frames n and m are such that the relative uncertainty in $|u|$ is approximately 4%. Values for n and m are 2–5.

Each experiment is at least repeated three times, and the values reported (velocities and time-to-horizontal) are averages of the multiple realizations. The error bars we present are the standard deviations of the repetitions. Their length is mostly consistent with the image analysis uncertainty estimates.

5 | COMPUTATIONAL SETUP

We have used an in-house developed lattice-Boltzmann flow solver based on a scheme proposed by Eggels and Somers[17] to perform fully-resolved simulations of a settling cylinder under conditions (in terms of Ar, l/d, and γ) within the ranges covered by the experiments. Details of the computational methodology are the same as used before to simulate the fluidization of cylindrical particles.[18] In summary: The method operates on a uniform cubic, three-dimensional mesh with lattice spacing Δ. We have an immersed boundary method (IBM) that imposes the no-slip condition at the surface of the cylinder. With a default lattice spacing of $\Delta = d/16$, we resolve the three-dimensional and time-dependent fluid flow around the cylinder. Each time step, the IBM determines the force and torque the fluid exerts on the cylinder. That information we use to update its linear and angular velocity in three dimensions through numerically solving Newton's second law and Euler's equations, respectively, as well as to update the location and orientation of the cylinder. For the orientation updates we use quaternions.[19] Quaternions are an elegant and efficient way to perform rotations in three-dimensional space. Once the angular velocities of an object are known, quaternions provide an exact solution of the change in orientation of the object over a time step Δt.

As noted, the default spatial resolution of the simulations is such that the diameter of a cylinder spans 16 lattice spacings: $\Delta = d/16$. The time step is such that $\Delta t = 4.33 \cdot 10^{-4}\sqrt{d/g}$. In order to assess grid effects, some simulation cases have been repeated on a coarser mesh with a larger time step: $\Delta = d/12$ and $\Delta t = 7.69 \cdot 10^{-4}\sqrt{d/g}$.

With the default resolution, we are not able to simulate the entire settling column. As an example: a cylinder with a diameter $d = 2$ mm has a grid with $\Delta = 0.125$ mm. To capture the entire column with this grid requires $640 \times 640 \times 6400 \approx 2.6 \cdot 10^9$ lattice cells, which is beyond our computational capabilities. Therefore, we use a smaller domain with fully periodic boundary conditions that is carefully force balanced.[20] As we will see, the wake behind the cylinder can get very long, so that we (still) need a tall domain, that is, a domain that is large in the vertical (=gravity) direction. The default domain size in the vertical direction is $150d$, in the horizontal direction

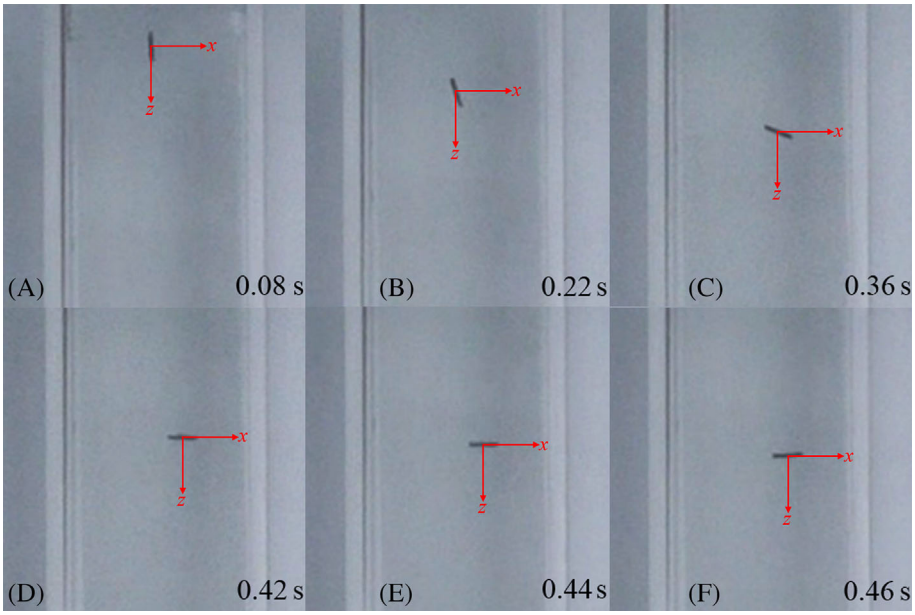

FIGURE 1 Sample camera frames of an experiment recorded at 50 fps of a $d = 1.97$ mm stainless steel cylinder falling through a 80% glycerol/20% water mixture. Six moments in time as indicated; $l/d = 6.75$ and Ar = 78.8

the size of the domain is at least $1.33l$.The initial condition of a simulation is zero fluid velocity everywhere and a zero velocity cylinder that is oriented almost vertically at the top of the (periodic) flow domain. To mimic the experiment we give the cylinder a small initial inclination angle of 0.5° with the vertical. We have checked the sensitivity with respect to this—quite arbitrary—choice and will report this in Section 6. The intention is to run simulations for as long as needed for the cylinder to reach a stable horizontal orientation. This has been achieved for all but the lowest Archimedes number (Ar = 4.83) that we investigated through simulation. Typically simulations cover of the order of $3 \cdot 10^5$ time steps. In physical terms, this means a simulated time of $130\sqrt{d/g}$. With $g \approx 10$ m/s^2 and, for example, $d = 2$ mm, this is a simulated time of the order of 2 s.

6 | RESULTS

Figure 1 shows sample camera frames of one of our settling experiments. The cylinder is released vertically and—as can be seen—rotates in the course of the experiment to a stable horizontal orientation. At $t \approx 0.44$ s ($tv/d^2 \approx 8.3$), the cylinder gets horizontal for the first time. We also see that beyond $t = 0.44$ s, the cylinder rotates slightly further.An impression of a simulation is given in Figure 2. It shows the cylinder and velocity magnitude contours in an xz cross-section in the middle of the entire computational domain, as well as detailed views of the cylinder and the flow around it at specific time instances. The figure makes it clear why one needs a tall domain. The wake behind the cylinder stretches out far in the vertical (z) direction. Given the fully periodic conditions, we want to avoid the cylinder to move through the wake of its downstream periodic copy. We also see the flow reaching the lateral domain boundaries.

It is already clear from the velocity contours that the fluid around the cylinder—and therefore the cylinder itself—slows down while rotating to horizontal. At the final snapshot (at $tv/d^2 = 23.4$), we see a horizontal cylinder with an approximately symmetric wake behind it.

The way the settling process proceeds over time as a function of the two main dimensionless input parameters (the Archimedes number Ar and the aspect ratio l/d) is illustrated in Figure 3. It shows a time series of the angle ψ the cylinder makes with the horizontal plane and the speed of the cylinder represented by its Reynolds number. The cylinder starts (close to) vertical and at zero velocity. It speeds up, reaches a maximum velocity, and then slows down. The slowing down coincides with the period of strongest rotation: the drag force on the cylinder increases as it flips to horizontal. Figure 3 illustrates

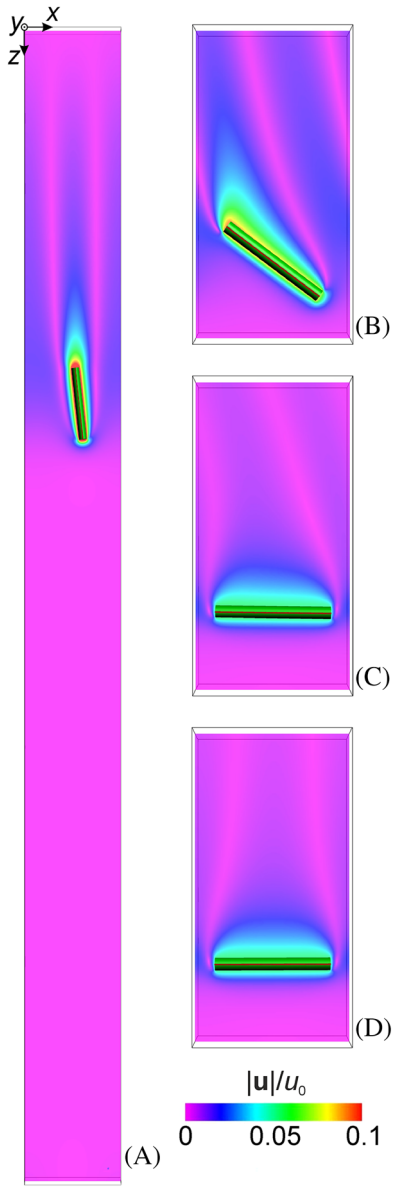

FIGURE 2 Simulation results for Ar = 77.3 and $l/d = 9.34$. (A) xz cross-section through the entire flow domain showing the cylinder and velocity magnitude contours at $tv/d^2 = 5.86$. (B)–(D) Detailed views of the cylinder and velocity magnitude at $tv/d^2 = 11.7$, 17.6, and 23.4, respectively. In the colour scaling, $u_0 = (\gamma - 1)d^2 g/v$.

two major dependencies. In the left column of frames of the figure, Ar increases from top to bottom while keeping l/d constant. It shows the transition from an almost monotonic decay of the orientation angle ψ (at Ar = 77.3) to a strongly damped wobbling (at Ar = 1240) to an almost undamped wobbling (at Ar = 19 800). The dimensionless (viscous) time scales on which this happens strongly depend on Ar.

In the right column of Figure 3, Ar is fixed and l/d decreases from top to bottom. The transition period from

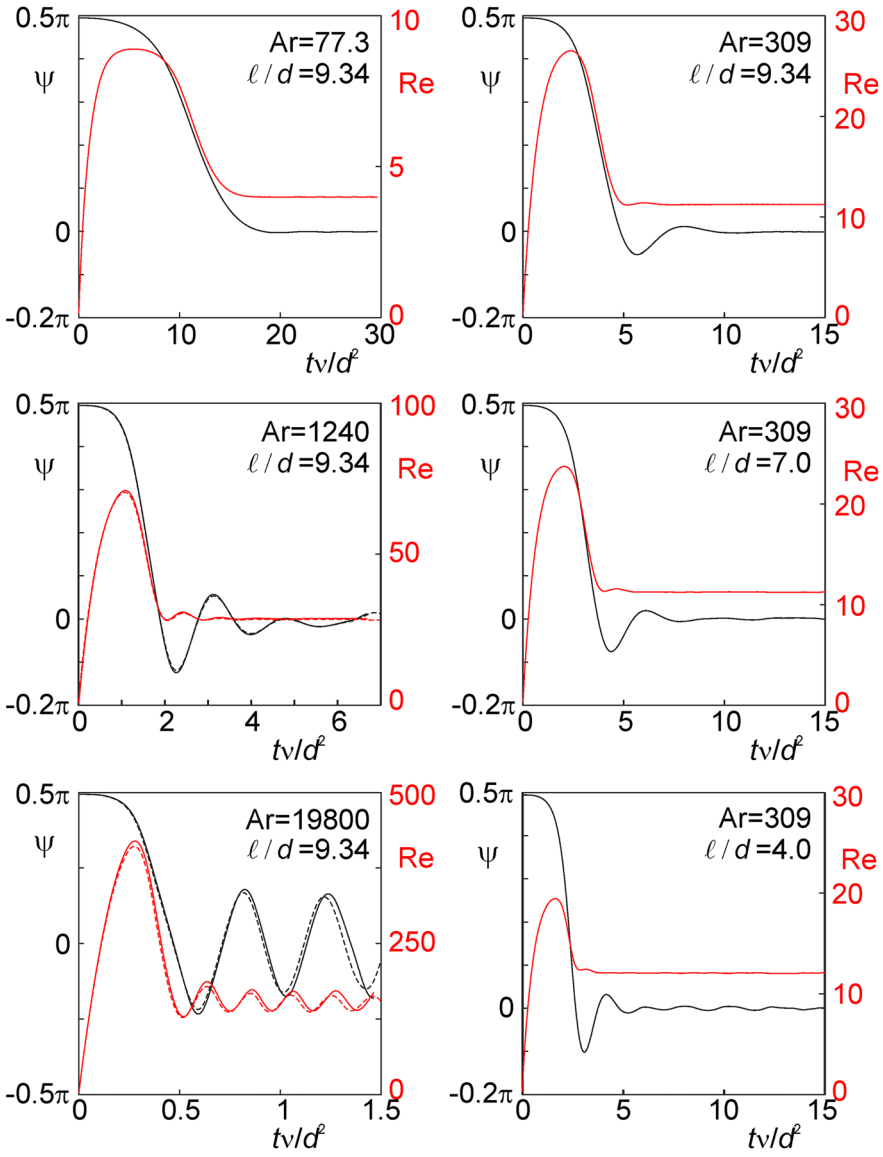

FIGURE 3 Simulation results: Time series of the angle ψ of the cylinder with the horizontal plane and Re for various Ar at one specific l/d (left) and at one Ar and various l/d (right). The dashed curves in the two lower left panels represent a lower spatial resolution of $\Delta = d/12$ as compared to the default $\Delta = d/16$.

vertical to horizontal is a function of l/d, with faster transitions for shorter cylinders. It is, however, interesting to note that at least for Ar = 309, the eventual settling velocity (Re number) only weakly depends on l/d. This can be understood by realizing that the net weight of the cylinder is proportional to its length l, and that also the drag force increases approximately linearly with l (we write 'approximately' given that end effects contribute to a diversion from linearity).

The two lower panels in the left column of Figure 3 assess the effects of the spatial resolution of the simulations with respect to the time history of orientation and settling speed. The dashed curves shown there are at a spatial resolution such that $d = 12\Delta$, whereas the default resolution (all solid curves in Figure 3) is $d = 16\Delta$. At Ar = 1240 the dashed and solid curves can hardly be distinguished which implies a well-resolved simulation at $d = 12\Delta$. At the higher Archimedes number of Ar = 19 800, t-he differences as a result of resolution are more apparent, the most visible effect being a slight reduction of the peak Reynolds number upon coarsening the mesh. At higher Archimedes numbers, Reynolds numbers increase and flow structures get finer which puts higher demands on spatial resolution.

In an experiment, a perfect vertical release of the cylinder is virtually impossible. In order to mimic this initial angle uncertainty in the simulations, by default the initial angle of the cylinder has been set to deviate by 0.5° from the vertical (in line with the discussion above about experimental uncertainty). The sensitivity of this choice of initial angle is investigated in Figure 4, top panel. It shows that the time scales of flipping depend on the initial condition with a very small angle of 0.1° delaying the time-to-horizontal by some 15% as compared to 0.5°. Obviously, the final, steady Reynolds number is independent of the initial cylinder orientation.

Another check shown in Figure 4 relates to the size of the computational domain, specifically its width. Here we compare a domain with $W/l = 1.34$ (default) with $W/l = 2.14$. There is an effect of domain width, specifically when it comes to the amplitude of wobbling fluctuations (in ψ as well as in Re). The narrower domain shows slightly lower amplitudes, which indicates that the periodic neighbours of the cylinder somewhat hinder/dampen its wobbling motion.

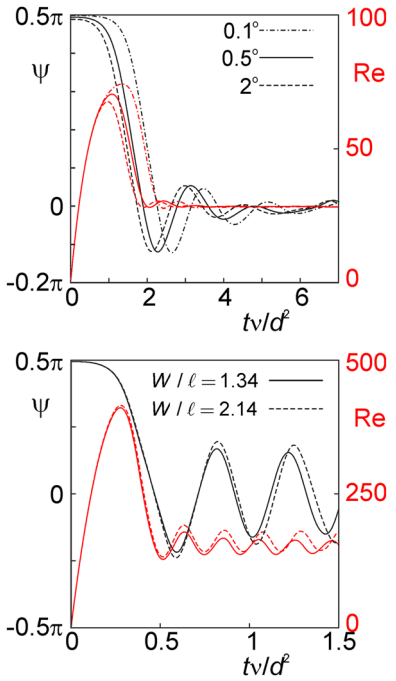

FIGURE 4 Simulation results. Time series of ψ and Re. Top: effect of the amount the initial angle deviates from the vertical (Ar = 1240, $l/d = 9.34$, $\Delta = d/12$). Bottom: effect of domain width (Ar = 19 800, $l/d = 9.34$, $\Delta = d/12$)

We now turn to confronting experimental and simulation results. Figure 5 shows the large extent of the set of experiments and the full range of Archimedes numbers that was investigated, $0.06 \leq \mathrm{Ar} \leq 308\,000$. It also shows the more limited set of simulations that were in the range $19 \leq \mathrm{Ar} \leq 7.9 \cdot 10^4$ (3.5 orders of magnitude). All simulations reported in this figure use the (default) spatial resolution of $d = 16\Delta$. As can be seen in Figure 5, the dimensionless time-to-horizontal $t\nu/d^2$ clearly depends on Ar. An increase of Ar by almost 6 orders of magnitude is associated with a decrease of $t\nu/d^2$ by 4–5 orders of magnitude. The experiments also show that, at a given Ar, $t\nu/d^2$ increases if l/d increases: a long cylinder takes more time to flip to horizontal than a short one.

The trends of $t\nu/d^2$ with Ar and l/d are well captured by the simulations. Carefully comparing simulations and experimental points in Figure 5 shows that the simulations slightly over-predict the experiments. We take a closer look at this is in Figure 6. Here, we used linear scales on the x and y-axis and have singled out experimental data with an Ar close to the simulations for which we investigated l/d effects: $\mathrm{Ar} \approx 300$, 1200, and 19 000. The trend of $t\nu/d^2$ increasing with l/d is now immediately clear in experiments and simulations. The extent to which the simulations overpredict the time-to-horizontal is in the range of 5%–20%.

Reynolds numbers are somewhat underestimated by the simulations (see the upper panels of Figure 6) but do show the same downward trend with l/d as the experiments. One should note the fairly limited reduction of Re with l/d. As mentioned above, increasing net gravity with increasing cylinder length also increases the drag force.

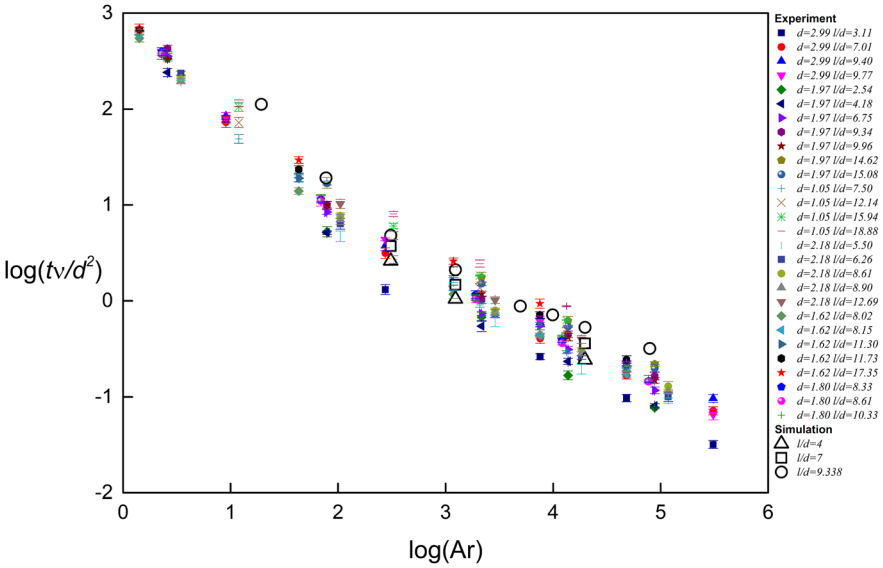

FIGURE 5 Comparison between experiments and simulations: Dimensionless time for the cylinder to get horizontal for the first time $t\nu/d^2$ versus the Archimedes number Ar. For the experimental data, the diameter d is given in mm in the legend.

Reynolds number data over the full range of Ar are presented in Figure 7. The narrow band of experimental points, much narrower than in Figure 5, shows that Re almost exclusively depends on Ar and not so much on l/d. Tentatively fitting a straight line through the experimental points in the double-logarithmic Figure 7 would describe the relationship between Re and Ar as $Re \approx 0.1\mathrm{Ar}^{2/3}$. It is relevant to compare the trends identified in Figure 7 with results presented in Toupoint et al.,[14] specifically their Figure 6. The latter figure also shows settling Reynolds numbers (now based on time-averaged velocity) as a function of Ar and l/d with their Archimedes number defined as $\sqrt{(\gamma-1)gd_e^3/\nu^2}$. The most striking difference between their Figure 6 and our Figure 7 is their strong dependency of the Reynolds number on the Archimedes number and the aspect ratio where we (see Figure 7) mostly see a dependency on Archimedes and not much on l/d. This difference largely comes down to the definition of the Archimedes number that we chose, such as to factor out the cylinder length; see the discussion in Section 2.

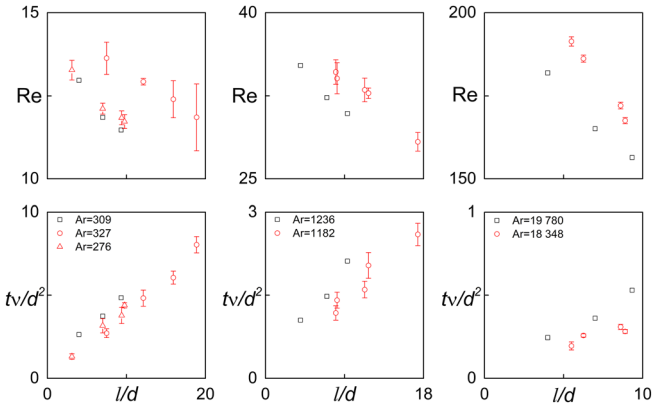

FIGURE 6 Comparison between experiments (red symbols) and simulations (black symbols). Top row: Reynolds number at the moment the cylinder is horizontal for the first time as a function of aspect ratio. Bottom row: dimensionless time for the cylinder to get horizontal. Archimedes numbers as indicated. The error bars represent one standard deviation on either side of the symbol.

The simulation results agree reasonably well with the experimental data over a wide range of Ar. We have been able to push the simulations into the high Archimedes number range and still have reasonable results for the Reynolds number (at the moment the cylinder gets horizontal) as well as for the dimensionless time-to-horizontal (as shown in Figure 5).

We hypothesize that the deviations between experiment and simulation are in a large part due to the need to limit the domain size in the simulations, as well as—at the high end of the Archimedes number range—limits to the spatial resolution. Ideally, we would have simulated the entire column as used in the experiment, including applying no-slip conditions at all bounding walls. As explained earlier, this is beyond our computational resources and we had to revert to smaller domains and periodic boundary conditions. In light of this, we have assessed in Figure 4 the effect of the domain width on the settling process and found relatively minor effects.

7 | CONCLUSIONS

Experiments and numerical simulations on cylinders settling through a quiescent Newtonian liquid have been performed. Variation of fluid viscosity, cylinder diameter, and cylinder density allowed for investigating

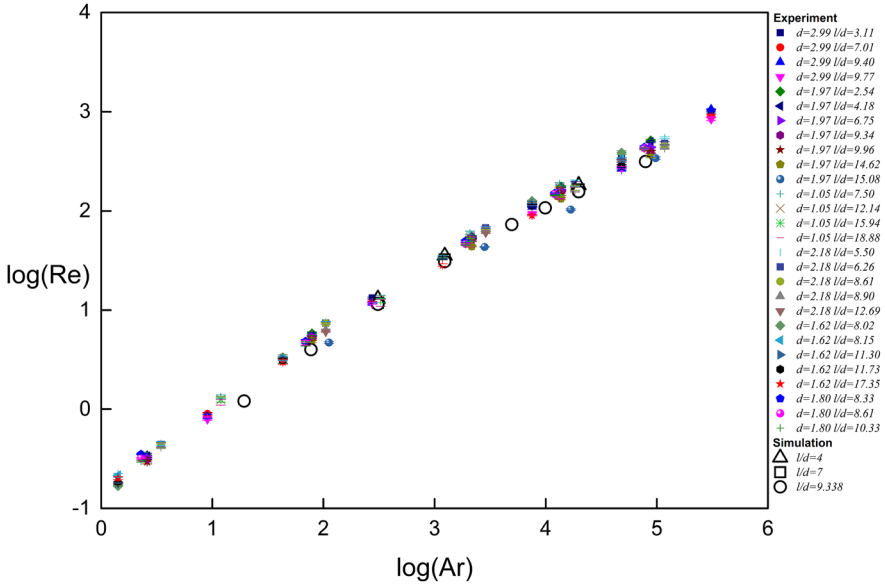

FIGURE 7 Comparison between experiments and simulations: Reynolds number at the moment the cylinder gets horizontal for the first time Re versus the Archimedes number Ar. For the experimental data, the diameter d is given in millimetre in the legend.

over a broad range of Archimedes numbers with $\mathrm{Ar} = (\gamma - 1)gd^3/\nu^2$. Length over diameter aspect ratios covered $2.5 \leq l/d \leq 20$. Cylinders were released vertically. The height of our flow system was such that in the grand majority of cases, the cylinders rotated and reached the bottom oriented horizontally. Dependent on Ar, this transition was associated with a wobbling motion of the cylinder. The two main output metrics of the experiment were the dimensionless time from release to reaching horizontal orientation for the first time $t\nu/d^2$, and the Reynolds number at that moment. An uncertainty analysis of these two measured quantities was performed based on the properties of our imaging system. We estimate a relative uncertainty of 8% and 4% in $t\nu/d^2$ and Re respectively. These values are aligned with uncertainties that were observed when repeating experiments.

With the definition of Ar as used in this paper, the Reynolds number is only weakly dependent on l/d and strongly depended on Ar. The dimensionless time decreases with increasing Ar and decreases with decreasing l/d.The experimental results were confronted with particle-resolved numerical simulations. The latter used periodic boundary conditions and an explicitly forced-balanced flow domain. The simulations were verified by assessing the effect of spatial resolution as well as domain size. Grid resolution effects clearly depend on Ar. Where at $\mathrm{Ar} \approx 10^3$ grid effects are negligible, at $\mathrm{Ar} \approx 2 \cdot 10^5$ they are well noticeable. The sensitivity of the dimensionless time-to-horizontal with respect to the cylinder orientation at release—which is hard to control in the experiment—was tested as well. The main trends with Ar and l/d were well represented by the simulations. We observe reasonable quantitative agreement between experiment and simulation in the metrics identified above. It is hypothesized that deviations in the Reynolds number partly relate to domain size effects.

Future work will develop along two lines: (1) refining the experiment; (2) extending the range of applications. In order to get a full view of the essentially three-dimensional motion of the cylinder, we plan to record the cylinder motion with two orthogonally placed camera's. This will allow us—for instance—to record time series of the angle between the cylinder centre line and the vertical direction.

In terms of applications, experimental work is planned for hollow cylindrical particles, as well as flexible cylinders. The latter with processing of fibres in applications such as biomass conversion and papermaking in mind. We have computational capabilities for flexible particles[21] so that this application will also be studied numerically. From a practical perspective, cylinder suspensions and, therefore, hydrodynamic interactions between cylinders are relevant topics of research. As a first step, we envisage well-controlled systems of two settling cylinders perturbing one another. Such systems can be studied experimentally and computationally with the aim of developing an experimentally validated computational approach to solid–liquid flow systems containing multiple cylinders.

AUTHOR CONTRIBUTIONS

Jinghan Xie: Conceptualization; data curation; investigation; validation; visualization; writing – original draft. **Lijuan Zhang:** Funding acquisition; writing – review and editing. **Menghua Lu:** Validation. **Jie Lu:** Resources; supervision. **Jos J. Derksen:** Data curation; formal analysis; methodology; software.

ACKNOWLEDGEMENTS

This work was supported by the National Natural Science Foundation of China (grant numbers: 22078191, 21978165, and 22081340412).

PEER REVIEW

The peer review history for this article is available at https://publons.com/publon/10.1002/cjce.24544.

DATA AVAILABILITY STATEMENT

Data available on request from the authors: The data that support the findings of this study are available from the corresponding author upon reasonable request.

ORCID

Lijuan Zhang https://orcid.org/0000-0001-5598-8691

REFERENCES

[1] M. Hartman, J. G. Yates, *Collect. Czech. Chem. Commun.* **1993**, *58*, 961.
[2] H. H. Hu, D. D. Joseph, M. J. Crochet, *Theor. Comput. Fluid Dyn.* **1992**, *3*, 285.
[3] J. Feng, H. H. Hu, D. D. Joseph, *J. Fluid Mech.* **1994**, *261*(1), 95.
[4] J. J. Derksen, R. A. Larsen, *J. Fluid Mech.* **2011**, *673*, 548.
[5] E. Loth, *Powder Technol.* **2008**, *182*, 342.
[6] G. B. Jeffery, *Proc. R. Soc. A* **1922**, *102*, 161.
[7] E. K. Marchildon, A. Clamen, W. H. Gauvin, *Can. J. Chem. Eng.* **1964**, *42*, 178.
[8] G. K. Youngren, A. Acrivos, *J. Fluid Mech.* **2006**, *69*, 377.
[9] M. Loewenberg, *Phys. Fluids A* **1993**, *5*(3), 765.
[10] M. Hyensjo, A. Dahlkild, *Int. J. Multiphase Flow* **2008**, *34*(9), 894.
[11] K. Chiba, K. W. Song, A. Horikawa, *Rheol. Acta* **1986**, *25*(4), 380.
[12] D. D. Joseph, J. Nelson, H. H. Hu, Y. J. Liu, in *Theoretical and Applied Rheology* (Eds: P. Moldenaers, R. Keunings), Elsevier, Belgium **1992**, p. 60.
[13] Y. J. Liu, D. D. Joseph, *J. Fluid Mech.* **1993**, *255*(1), 565.
[14] C. Toupoint, P. Ern, V. Roig, *J. Fluid Mech.* **2019**, *866*, 82.

[15] P. Romero-Gomez, M. C. Richmond, *Journal of Fluids and Structures* **2016**, *61*, 154.
[16] R. Clift, J. R. Grace, M. E. Weber, *Bubbles, Drops, and Particles*, 1st ed., Academic Press, New York **1978**.
[17] J. G. M. Eggels, J. A. Somers, *Int. J. Heat Fluid Flow* **1995**, *16*(5), 357.
[18] J. J. Derksen, *AIChE J.* **2019**, *65*, e16594.
[19] J. B. Kuipers, *Quaternions and Rotation Sequences*, Princeton University Press, Princeton, NJ **1999**.
[20] J. J. Derksen, S. Sundaresan, *J. Fluid Mech.* **2007**, *587*, 303.
[21] J. J. Derksen, *AIChE J.* **2020**, *66*, e16952.

How to cite this article: J. Xie, L. Zhang, M. Lu, J. Lu, J. J. Derksen, *Can. J. Chem. Eng.* **2023**, *101*(4), 2240. https://doi.org/10.1002/cjce.24544